Supplementary Information for

Polar amplification of Pliocene climate by elevated trace gas radiative forcing

P. Hopcroft, G. Ramstein, T. Pugh, S. Hunter, F. Murguia-Flores, A. Quiquet, Y. Sun, N. Tan and P. Valdes

Peter Hopcroft:
E-mail: p.hopcroft@bham.ac.uk

This PDF file includes:

www.pnas.org/cgi/doi/10.1073/pnas.2002320117

Supporting Information Text

Climate model simulations of the Pliocene

The four GCMs used in this study encompass the spread of climate sensitivities amongst the models in PlioMIP (1), see table S2. Each model uses CMIP5 pre-industrial boundary conditions, except HadCM3-M21 which is described by (2), but which is very similar. For the Pliocene, IPSL-CM5A-LR Pliocene simulations are available with both PlioMIP phase 1, experiment 2 (3) and PlioMIP phase 2 Eoi^{400} (4) boundary conditions. HadCM3 uses PlioMIP phase 2 Eoi^{400} boundary conditions (5). We also include Pliocene simulations with HadCM3 that are identical to Eoi^{400} except the CO_2 mixing ratio is set to 450 or 490 ppmv, see table S2. CCSM4 and GISS-E2-R are the PlioMIP phase 1 simulations by (6) and (7), respectively.

Pre-industrial simulations are as submitted to the Coupled Model Intercomparison Project phase 5 (CMIP5), except for HadCM3 for which the setup is very similar (5). In the IPSL and CCSM4 PlioMIP phase 1 simulations the land-sea mask was not altered from its pre-industrial configuration, but the orography, ice sheets and vegetation coverage follow the PRISM3 reconstruction for the Pliocene (3, 6). In CCSM4 the Hudson Bay is infilled with land. GISS incorporates the PRISM3 Pliocene boundary conditions for orography, sea-level, land-sea mask and vegetation coverage (7). In the PlioMIP phase 2 simulations HadCM3 and IPSL use the PRISM4 reconstructions of orography, land-sea-mask, ice sheet and vegetation (4, 5). HadCM3 also incorporates reconstructed Pliocene soil types and lake areas.

We compare the JJA temperature and precipitation anomalies in the 5 pairs of GCM simulations in figure S2. All models show strongest warming in the northern hemisphere focussed on the North Atlantic. HadCM3 warms the most substantially, especially over land and in the northern hemisphere extra-tropics. The introduction of changes to orography and land sea mask in PlioMIP phase 2 lead to additional warming compared to PioMIP1 in the IPSL model, but the magnitude is around 0.5-1. Comparisons with reconstructions are shown for HadCM3 in figure 3 of the main text and figure S3, and for the IPSL model in figure S4.

Most models predict enhanced rainfall in North Africa and South East Asia, but the signal over tropical South America is divergent with either drier (HadCM3, CCSM4, IPSL-Eoi^{400}) or slightly wetter conditions (GISS, IPSL-PlioMIP phase 1). The precipitation signal in the extra-tropics is also quite variable, with IPSL simulating drier conditions in North America and with other models showing more complex patterns, except for HadCM3 which shows a clear drying signal over Europe.

LPJ-GUESS simulations

LPJ-GUESS uses 12 plant functional types (PFTs) and 25 replicate patches within each gridcell. These represent the distribution of stand histories in terms of disturbance and succession. The establishment and mortality of age cohorts of PFTs are represented stochastically across these patches. The GCM climate inputs are surface air temperature, precipitation, surface downwelling short-wave radiation, number of days per month with precipitation >0.1 mm, and minimum and maximum daily temperature.

Emissions modelling

Wetland methane. Wetland CH_4 emissions are calculated following (8) as:

$$E_{CH_4} = k_{CH4} F_{wet} S_c Q_{10}(T)^{0.1(T-T_0)}, \quad [1]$$

where F_{wet} is the wetland fraction in a given gridcell as calculated below, T_0=0 K, $Q_{10}(T_0)$ is 3.9 following (9), S_c is soil carbon from LPJ-GUESS and k_{CH4} is adjusted for different GCM simulations, so that the pre-industrial global flux is 140 $TgCH_4$/yr in each case.

The TOPMODEL formulation is based on the relationship between the local and large-scale water table depth and the topographic index:

$$z_i = \overline{z} + \frac{1}{f}(TI_i - \overline{TI}) \quad [2]$$

where z is the water table depth and TI is the topographic index and is equal to $ln(\alpha/tan(\beta))$, where α is the drainage area and tanβ is the local topographic slope (e.g. 10). We use values from (11) expanded to LGM continental shelves using ETOPO1 observations (12), to allow for changes in land area during the Pliocene relative to today. The subscript i refers to the local or subgrid values, and overbars represent large scale (or GCM resolution gridbox) mean values. The topographic index allows determination of the fractional coverage in a gridcell at a certain water

table depth. This relies on defining the subgrid-scale values of TI. In practice this is achieved by approximating the observations with a probability density function, for which we use a two parameter exponential function (13). This greatly simplifies the overall computation, leading to an area F_{sat} with a water table at or above the surface given by:

$$F_{sat} = F_{max} e^{(-C_s f(z_i - \overline{z}))} \quad [3]$$

where f is the parameter relating the exponential decline in hydrologic transmissivity with depth. Here this parameter is chosen to give a similar global mean wetland area in the pre-industrial simulations with different driving climatologies. The gridcell mean water table depth $\overline{z}$ is calculated from the grid-cell mean water content following (14), and for saturated conditions, z_i is equal to zero. F_{max} is the fraction of the gridcell for which sub-grid values of $TI_i \geq \overline{TI}$ (13), and is calculated at each coarse resolution grid-cell from the 15 arcsec resolution topographic index data of (11). Following (15) and (16), to calculate F_{wet} in equation 1, a maximum topographic index is assumed, so that in equation (3), F_{max} is replaced by F^{wet}_{max}, which is the fraction of each grid-cell with high-resolution $TI_i \geq \overline{TI}$ and $TI_i \leq TI_{max}$, where TI_{max}=12.0. Sub-grid areas with TI_i greater than this threshold are assumed to contain running water or to have a water table position above the soil surface that allows methanotropy. C_s is calculated by fitting an exponential function to the sub-gridcell values of topographic index (where the values exceed the gridcell mean) following (13, 17). C_s is then modified based on the January surface air temperature following (18).

Wetland area is configured to give a pre-industrial area in the range 13.6±4.8 x10^6 km^2. This is based on the multi-study mean present day wetland area from the five most recent studies summarised by (19) of 10.5±3.7 x10^6 km^2, which is augmented by 30% to account wetland area loss since the late Holocene pre-industrial, estimated as between 34-50% (20–22).

Other Trace gas emissions. The soil NOx model(23) requires soil moisture and temperature, soil nitrogen and rainfall return periods all of which are estimated based on the GCM outputs. We parameterise the rainfall return period as a function of wetdays, with a maximum return period of 10 days. This produces a pre-industrial emissions distribution that is consistent with the results from other modelling studies.

Parametric atmospheric CH_4 lifetime model description and validation

The parametric model has the functional form:

$$log(\tau_{CH_4 \times OH}(t)) = log(\tau_{CH_4 \times OH}(t_0)) + \Sigma_i \alpha_i \Delta log[F_i(t)] \quad [4]$$

where τ is CH_4 lifetime, α_i is the sensitivity factor for variable i defined in table 2 by (24), ΔF_i is the change in variable i, t is the time period of interest and t_0 represents pre-industrial or present day control conditions. Here $\tau(t_0)$ is set to 10.4 years, and we calculated α=0.275 for total isoprene and monoterpene emissions based on simulations by (25). Water vapour change is calculated from the global mean temperature increase assuming it increases at a rate of 5.7%/K.

We validate this with published results for the Pliocene from (26). This results in a lifetime increase by 4.3 years, which is slightly exceeds the simulated change of 4.1 years reported for full chemistry-transport model simulation (for CH_4=1500 ppbv), see the supporting information table S3. However, this value is within the uncertainty limits of the calculation of 3.2-5.5 years.

Radiative forcing by atmospheric CH_4

The direct methane radiative forcing is approximately 0.58±0.16 Wm^{-2} per 1000 ppbv having been revised upwards by 15% (27). Because of its short lifetime, CH_4 also influences the levels of ozone, water vapour, and sulphate aerosols. These interactions induce additional radiative forcing contributions which are given in table S4. For this we assume that the dependence of O_3 production from CH_4 on the present-day background level of NOx can also be applied in the pre-industrial and Pliocene, which does not seem too unrealistic (28). We also assume that indirect CH_4-SO_4 effects are not important in the pre-anthropogenic atmosphere.

Comparison with temperature reconstructions

Figure 3 in the main text and figure S3 compare simulated and reconstructed changes in near-surface air temperatures (ΔT) and sea-surface temperature (ΔSST), respectively for HadCM3. An equivalent analysis for IPSL is shown in figure S4. Reconstructed (ΔT) anomalies are from (29) and are relative to CRUT3.22 1961-1990 climatology (30). For the ΔT, we include the reported bioclimatic range uncertainties. Reconstructed ΔSST anomalies and three standard deviation uncertainties are from Foley & Dowsett, 2019 (31) and are relative to HadISST 1871-1920 climatology (32).

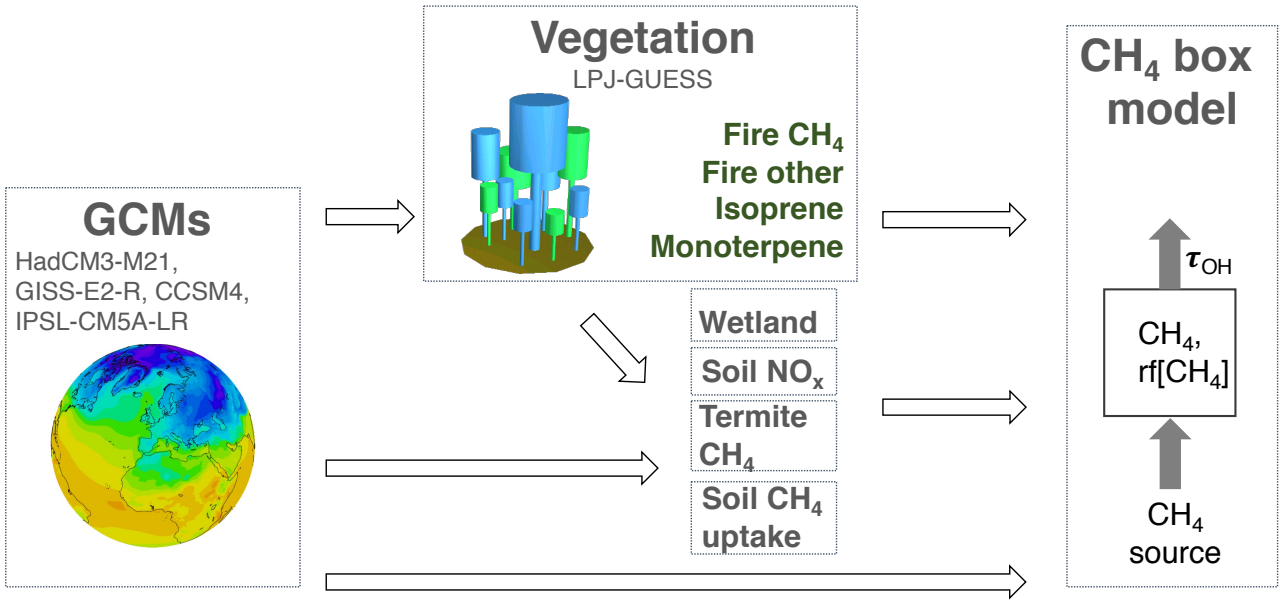

Fig. S1. Schematic of the overall modelling framework.

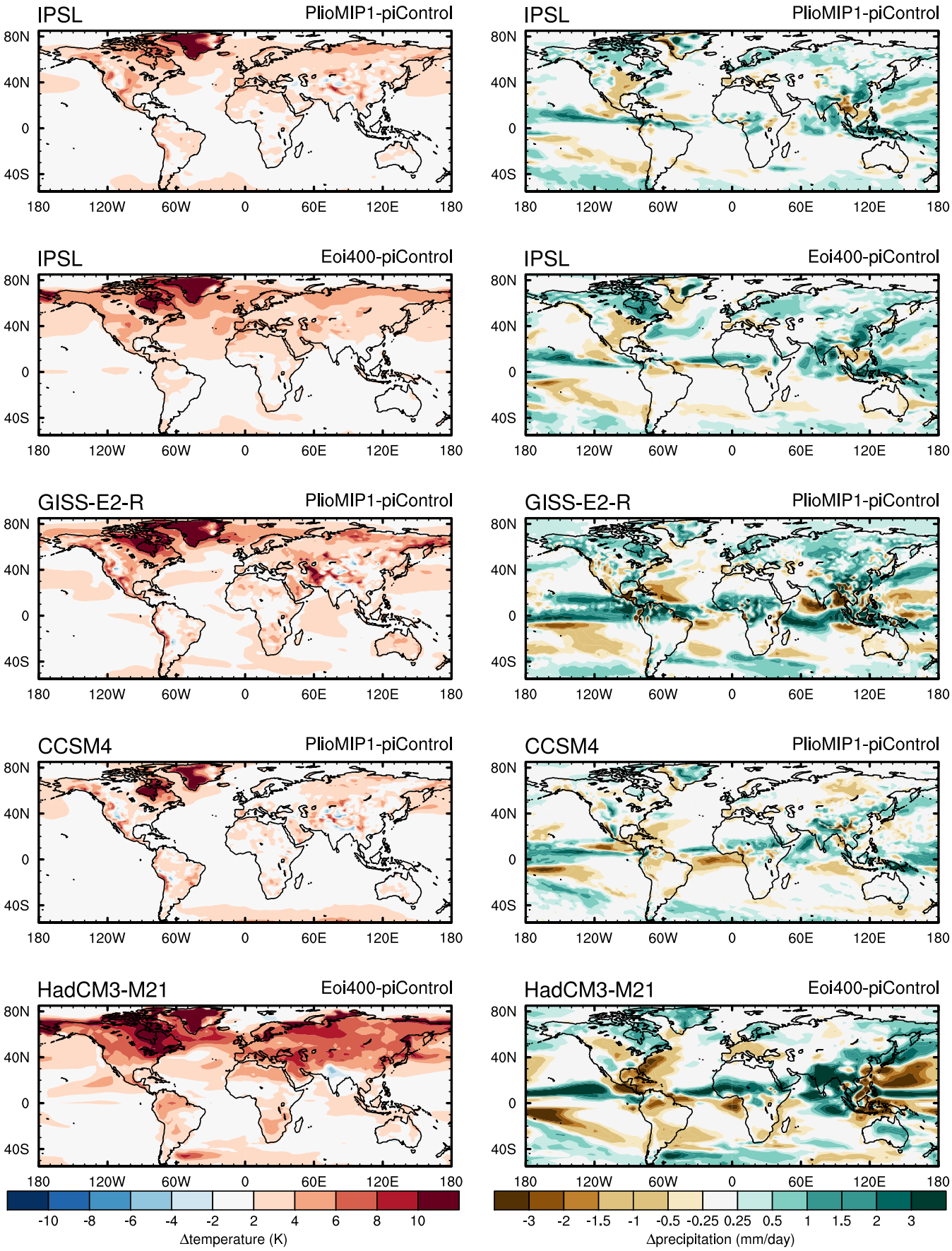

Fig. S2. JJA Pliocene minus pre-industrial anomalies of surface air temperature (left: °C) and precipitation (right: mm/day). JJA anomalies are shown because wetlands are more productive in the warm season and most extra-tropical wetlands are in the Northern Hemisphere.

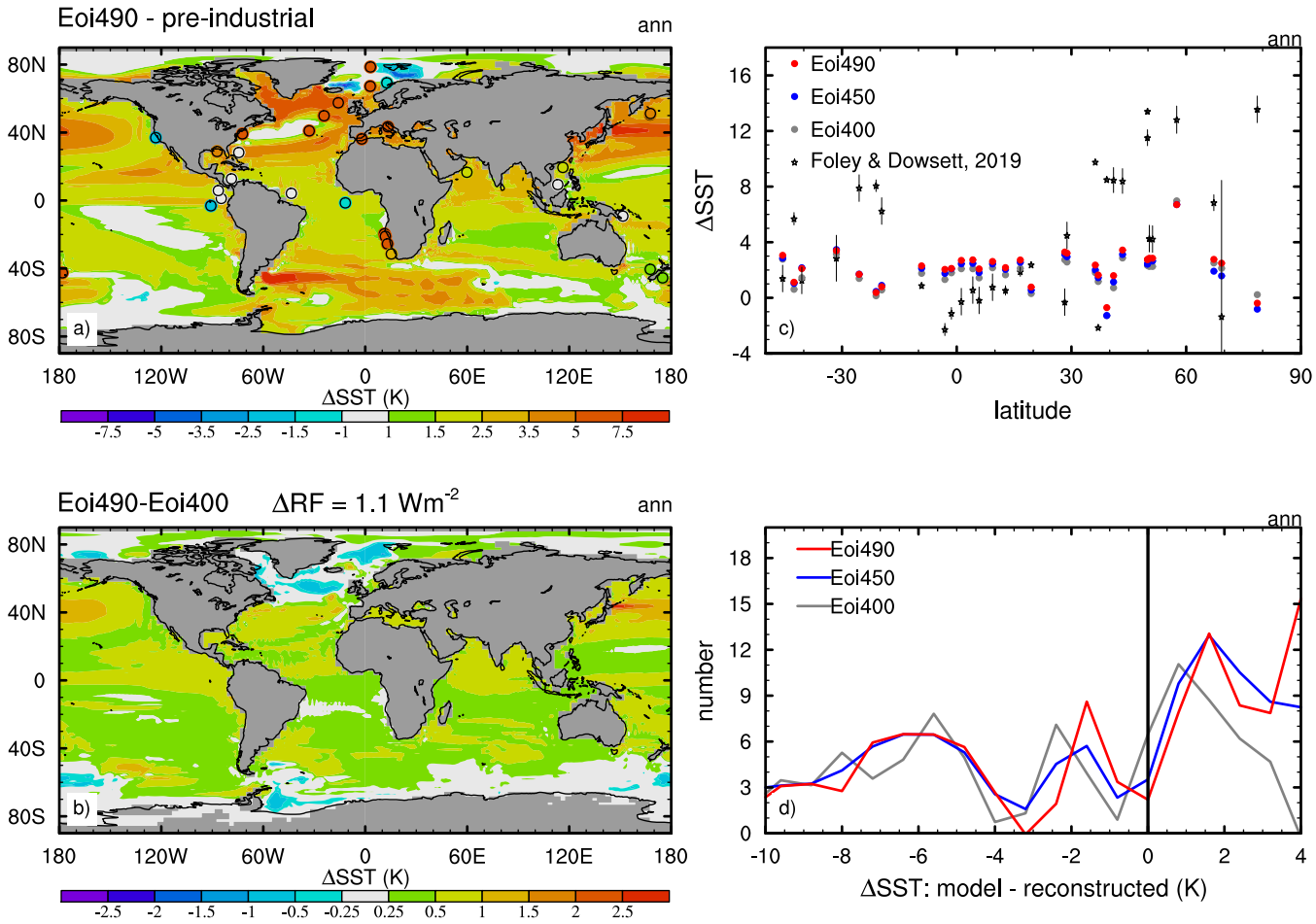

Fig. S3. Simulations with HadCM3-M21 and reconstructions of Pliocene sea surface temperature change (ΔSST) relative to the pre-industrial. (a)Simulated (5) and reconstructed (31, 33) ΔSST for Eoi490-pre-industrial, (b) simulated ΔSST for Eoi^{490} - Eoi^{400}, (c) latitudinal comparison of the reconstructed and simulated temperature anomalies, (d) histogram of model minus reconstruction anomalies.

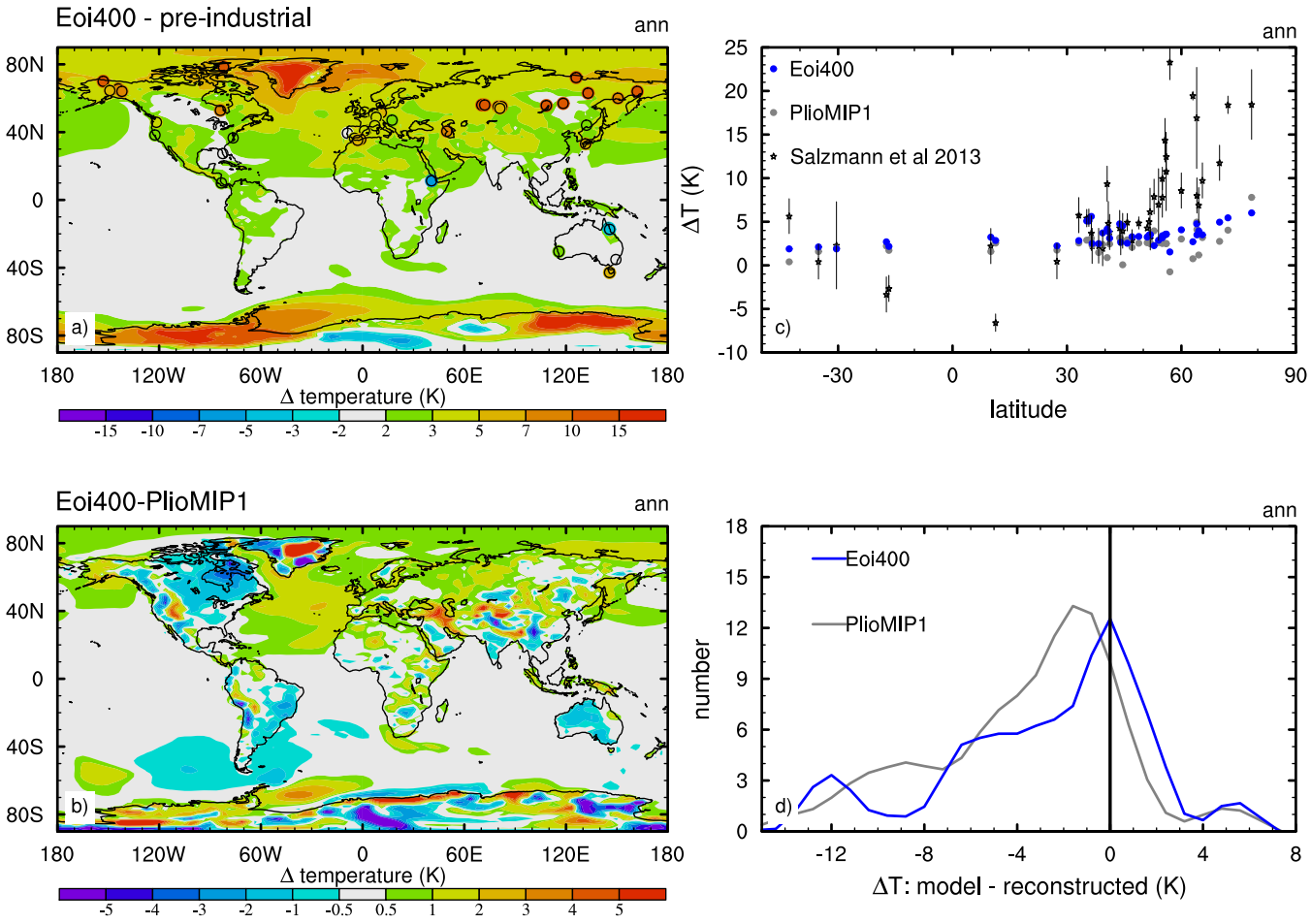

Fig. S4. As in figure 3, but for the PlioMIP phase 1 and Eoi^{400} simulations with IPSL-CM5A-LR.

Table S1. Global mean climate variables and fluxes of methane, non-methane volatile organic compounds (NMVOCs), nitrous oxides (NOx) and carbon from natural sources as simulated by LPJ-GUESS and other offline models forced with GCM climate fields for pre-industrial and Pliocene with atmospheric CO_2 of 280 and 400 ppmv, respectively. Pre-industrial fluxes are all normalised to the same four-model average to facilitate comparisons. The remaining CH_4 fluxes are assumed not to change during the Pliocene and comprise geological (10 Tg/yr), hydrates (10 Tg/yr) and oceans (1 Tg/yr). The fluxes from UY14 (26) are normalized to the pre-industrial fluxes used in this study.

GCM	-	HadCM3	IPSL-CM5A	IPSL-CM5A	CCSM4	GISS-E2-R	GISS-E2-R
Simulation	PI	Eoi^{400}	PlioMIP1	Eoi^{400}	PlioMIP1	PlioMIP1	PlioMIP1
Study	This study						UY14
CO_2	280	400	400	400	400	400	400
Climate variables							
ΔSurface air temperature ($^{\circ}$C)	-	2.9	2.2	2.3	1.8	1.9	2.4
ΔSurface humidity (%)	-	17.4	13.0		10.5	11.1	14.1
Methane cycle (emissions in $TgCH_4$/year)							
Wetlands	140	205	168	171	172	188	-
Wetland area ($\times 10^6$km^2)	15.7	16.8		15.7	15.6	17.4	-
Wildfires	21	34.7	38.0	38.6	32.5	31.6	-
Termites	20	27.4	25.0	24.8	24.3	24.1	-
Soil uptake (pCH_4=715 ppbv)	11	11.9	14.1	14.1	12.0	10.9	-
Net land source	191	267	238	241	237	254	-
Vegetation NMVOCs (TgC/year)							
Isoprene	689	968	947	926	776	723	1030
Monoterpene	117	119	120	125	110	112	101
Other fluxes							
Wildfire Carbon flux (TgC/yr)	4110	6793	7439	7563	6359	6185	8293
Soil NOx (TgN/yr)	9.0	8.4	10.6	10.5	11.6	11.7	12.9
Lightning NOx (TgN/yr)	6.7	-	-	-	-	-	7.6

Table S2. GCMs used in this study: equilibrium climate sensitivity (ECS), model resolution, original model reference and Pliocene simulation reference and global mean temperature anomaly relative to the pre-industrial simulation.

GCM	ECS (°C)	Institute	Resolution atmosphere/ocean (gridpoints, levels)	Model reference	Pliocene setup	Pliocene ΔT (°C)	Pliocene reference
CCSM4	3.2	NCAR, USA	288×192×L24 /384×320×L60	Gent et al. 2011 (34)	PlioMIP1: Exp. 2	1.8	Rosenbloom et al. 2013 (6)
GISS-E2-R	2.7	NASA-GISS, USA	144×90×L40 /144×90×L32	Schmidt et al. 2013 (35)	PlioMIP1: Exp. 2	1.9	Chandler et al. 2013 (7)
IPSL-CM5A-LR	3.4	IPSL, France	96×95×L39 /182×149×L31	Dufresne et al. 2013 (36)	PlioMIP1: Exp. 2	2.2	Contoux et al. 2012 (3)
					PlioMIP2: Eoi^{400}	2.3	Tan et al. 2020 (4)
HadCM3-M21	3.1	U. Leeds, UK	96×73×L19 /288×144×L20	Gordon et al. 2000, Valdes et al. 2017 (2, 37)	PlioMIP2: Eoi^{400}	2.9	Hunter et al. 2019 (5)
					PlioMIP2: Eoi^{450}	3.4	Hunter et al. 2019 (5)
					PlioMIP2: Eoi^{490}	3.6	This study

Table S3. Wetland emissions and factor separation. Pliocene simulations in which either surface temperatures, soil moisture or soil carbon are prescribed with pre-industrial (PI) values.

Methane emissions ($TgCH_4$/year)					
	pre-industrial	Pliocene			
GCM			PI temperature	PI soil moisture	PI soil carbon
CCSM4	140	172	141	173	166
GISS	140	188	160	173	198
ISPL (PlioMIP1)	140	168	131	170	173
ISPL (PlioMIP2)	140	171	128	173	178
HadCM3	140	205	135	156	247

Table S4. Terms in radiative forcing (mWm^{-2}/ppbv) calculation and their uncertainties (24). The direct effect is based on the work of Etminan et al.(27). Uncertainty estimates from literature (24) or prescribed at 20%. The total is consistent or even lower than estimates from other studies. For example Shindell et al. (38) simulated a value of 1.03 mWm^{-2}/ppbv, for an emissions-based radiative forcing of 0.99 Wm^{-2} and a concentration increase from CE 1750-2000 (around 750 ppbv to 1773 ppbv).

	Direct	O_3 from CH_4	O_3 from CH_4 via H_2O	H_2O from CH_4	Total
Mean (mWm^{-2}/ppbv)	0.55	0.232	-0.037	0.055	0.80
$\pm$1 s.d.	14%	21%	20%	20%	0.09

Table S5. Example calculation with equation 4 of the CH_4 lifetime for the Pliocene relative the pre-industrial based on simulated global mean changes reported by (26). The coupled climate-chemistry model change is 4.1 years from a pre-industrial value of 14.7 years.

F_i	ΔF_i	units	α_i	1σ	$\Delta\tau(yr)$	$\Delta\tau(\%)$
temperature	2.4	K	-3.0	0.8	-0.4 (-0.5,0.3)	-2.5
humidity	14.1	%	-0.3	0.03	-0.6 (-0.6,-0.5)	-3.9
column ozone	5	%	0.55	0.11	0.4 (0.3,0.5)	2.9
lightning NOx	13	%	-0.16	0.06	-0.3 (-0.4,-0.2)	-1.9
wildfires	100	%	0.02	0.015	0.2 (0.10.4)	1.4
CH_4	110	%	0.31	0.04	3.8 (3.3,4.4)	25.8
NMVOCs	31	%	0.275	10%	1.1 (1.0,1.3)	7.8
Soil NOx	42	%	-0.14	0.03	-0.7 (-0.9,-0.6)	-4.8
Total	-	-	-	-	4.4 (3.2,5.5)	30 (22,37)

References

1. AM Haywood, H Dowsett, AJ Dolan, D Rowley, et al. The Pliocene Model Intercomparison Project (PlioMIP) Phase 2: scientific objectives and experimental design. *Clim Past*, 12:663–675, 2016.
2. PJ Valdes, E Armstrong, M Badger, C Bradshaw, F Bragg, M Crucifix, T Davies-Barnard, J Day, A Farnsworth, C Gordon, PO Hopcroft, A Kennedy, N Lord, D Lunt, A Marzocchi, L Parry, V Pope, W Roberts, E Stone, G Tourte, and J Williams. The BRIDGE HadCM3 family of climate models: HadCM3@Bristol v1.0. *Geosci Model Dev*, 10:3715–3743, 2017.
3. C Contoux, G Ramstein, and A Jost. Modelling the mid-Pliocene Warm Period climate with the IPSL coupled model and its atmospheric component LMDZ5A. *Geosci Model Dev*, 5:903–917, 2012.
4. N Tan, C Contoux, G Ramstein, Y Sun, C Dumas, P Sepulchre, and Z Guo. Modeling a modern-like pCO2 warm period (Marine Isotope Stage KM5c) with two versions of an Institut Pierre Simon Laplace atmosphere,Äìocean coupled general circulation model. *Climate Past*, 16, 2020.
5. S Hunter, AM Haywood, AM Dolan, and JC Tindall. The HadCM3 contribution to PlioMIP Phase 2. *Clim Past*, 15:1691–1713, 2019.
6. NA Rosenbloom, BL Otto-Bliesner, EC Brady, and PJ Lawrence. Simulating the mid-PlioceneWarm Period with the CCSM4 model. *Geosci Model Dev*, 6:549–561, 2013.
7. M Chandler, L Sohl, J Jonas, H Dowsett, and M Kelley. Simulations of the mid-PlioceneWarm Period using two versions of the NASA/GISS ModelE2-R Coupled Model. *Geosci Model Dev*, 6:517–531, 2013.
8. N. Gedney, P.M. Cox, and C. Huntingford. Climate feedback from wetland methane emissions. *Geophys. Res. Lett.*, 31(L20503), 2004.
9. E Comyn-Platt, G Hayman, C Huntingford, et al. Carbon budgets for 1.5 and 2 °C targets lowered by natural wetland and permafrost feedbacks. *Nature Geoscience*, 11(568-573), 2018.
10. K. Beven and M. Kirkby. A physically based variable contributing area model of basin hydrology. *Hydrol Sci Bull*, 24:43–69, 1979.
11. TR Marthews, SJ Dadson, B Lehner, S Abele, and N Gedney. A high-resolution global dataset of topographic index values for use in large-scale hydrological modelling. *Hydrol Earth Syst Sci*, 19:91–104, 2015.
12. PO Hopcroft and PJ Valdes. Last Glacial Maximum constraints on the Earth System model HadGEM2-ES. *Climate Dynamics*, 45(5):1657–1672, 2015.
13. G Niu et al. A simple TOPMODEL-based runoff parameterization (SIMTOP) for use in global climate models. *J Geophys Res*, 110, 2005.
14. KW Oleson et al. Technical description of the Community Land Model (CLM). Technical report, 2004.
15. N Gedney and PM Cox. The sensitivity of global climate model simulations to the representation of soil moisture heterogeneity. *J Hydrometeorol*, 4:1265–1275, 2003.
16. T Kleinen, V Brovkin, and RJ Schuldt. A dynamic model of wetland extent and peat accumulation: results for the Holocene. *Biogeosciences*, 9:235–248, 2012.
17. Z Zhang, NE Zimmermann, JO Kaplan, and B Poulter. Modeling spatiotemporal dynamics of global wetlands: comprehensive evaluation of a new sub-grid TOPMODEL parameterization and uncertainties. *Biogeosciences*, 13:1387–1408, 2016.
18. Y Fan and G Miguez-Macho. A simple hydrologic framework for simulating wetlands in climate and earth system models. *Clim Dyn*, 37:253–278, 2011.
19. NC Davidson, E Fluet-Chouinard, and CM Finlayson. Global extent and distribution of wetlands: trends and issues. *Marine & Freshwater Research*, 69(4):620–627, 2018.
20. JB Zedler and S Kercher. Wetland resources: status, trends, ecosystem services, and restorability. *Ann Rev Environ*, 30:39–74, 2005.
21. NC Davidson. How much wetland has the world lost? Long-term and recent trends in global wetland area. *Marine & Freshwater Research*, 65:934–941, 2014.
22. R Paudel, NM Mahowald, PG Hess, L Meng, and WJ Riley. Attribution of changes in global wetland methane emissions from pre-industrial to present using CLM4.5-BGC. *Env Res Lett*, 11(034020), 2016.
23. R Hudman et al. Steps towards a mechanistic model of global soil nitric oxide emissions: implementation and space based-constraints. *Atmos Chem Phys*, 12:7779–7795, 2012.
24. CD Holmes, MJ Prather, OA Sovde, and G Myhre. Future methane, hydroxyl, and their uncertainties: key climate and emission parameters for future predictions . *Atmos Chem Phys*, 13:285–302, 2013.
25. P.J. Valdes, D.J. Beerling, and C.E.. Johnson. The ice age methane budget. *Geophys. Res. Lett.*, 32(L02704), 2005.
26. N Unger and X Yue. Strong chemistry-climate feedbacks in the Pliocene. *Geophys Res Lett*, 41(527-533), 2014.
27. M Etminan, G Myhre, EJ Highwood, and KP Shine. Radiative forcing of carbon dioxide, methane, and nitrous

oxide: A significant revision of the methane radiative forcing. *Geophys Res Lett*, 43:12614–12623, 2017.
28. O Wild and P Palmer. How sensitive is tropospheric oxidation to anthropogenic emissions? *Geophys Res Lett*, 35:L22802, 2012.
29. U Salzmann, AM Dolan, AM Haywood, et al. Challenges in quantifying Pliocene terrestrial warming revealed by data-model discord. *Nature Climate Change*, 3:969–974, 2013. .
30. I Harris, PD Jones, TJ Osborn, and DH Lister. Updated high-resolution grids of monthly climatic observations - the CRU TS3.10 Dataset. *Int J Climtol*, 34:623–642, 2014.
31. KM Foley and HJ Dowsett. Community sourced mid-Piacenzian sea surface temperature (SST) data. *U.S. Geological Survey data release, doi: 10.5066/P9YP3DTV*, 2019.
32. NA Rayner, DE Parker, EB Horton, CK Folland, LV Alexander, DP Rowell, EC Kent, and A Kaplan. Global analyses of sea surface temperature, sea ice, and night marine air temperature since the late nineteenth century. *J Geophys Res*, 108:D14,4407, 2003.
33. HJ Dowsett et al. Sea surface temperature of the mid-Piacenzian ocean: a datamodel comparison. *Scientific Reports*, 3, 2013.
34. PR Gent et al. The Community Climate System Model Version 4. *J Climate*, 24:4973–4991, 2011.
35. G Schmidt et al. Configuration and assessment of the GISS ModelE2 contributions to the CMIP5 archive. *J Adv Model Earth Syst*, 6, 141–184, 2013.
36. J-L Dufresne et al. Climate change projections using the IPSL-CM5 Earth System Model: from CMIP3 to CMIP5. *Clim Dyn*, 40(2123-2165), 2013.
37. C. Gordon, C. Cooper, C. A. Senior, H. Banks, J. M. Gregory, T. C. Johns, J. F. B. Mitchell, and R. A. Wood. The simulation of sst, sea ice extents and ocean heat transports in a version of the Hadley Centre coupled model without flux adjustments. *Climate Dynamics*, 16(2-3):147–168, 2000.
38. D Shindell et al. Improved attribution of climate forcing to emissions. *Science*, 326:716–718, 2009.